Sensors and Materials, Vol. 32, No. 4 (2020) 1389–1394
MYU Tokyo

S & M 2185

Scintillation Properties of Ti- and Zr-doped $Gd_2Hf_2O_7$ Crystals

Daisuke Nakauchi,* Takumi Kato, Noriaki Kawaguchi, and Takayuki Yanagida

Division of Materials Science, Nara Institute of Science and Technology (NAIST),
8916-5 Takayama, Ikoma, Nara 630-0192, Japan

(Received December 21, 2019; accepted March 10, 2020)

Keywords: scintillator, radioluminescence, phosphor, dosimetry, pyrochlore

Zr-doped and Ti-doped $Gd_2Hf_2O_7$ single crystals were synthesized by the optical floating zone (FZ) technique to evaluate their scintillation properties. The synthesized single crystals show scintillation signals with a broad peak at 510 nm, and scintillation decay curves consist of two exponential functions with decay time constants on the nanosecond order. Both the Ti and Zr doping processes seem to enhance the scintillation properties of $Gd_2Hf_2O_7$. Regarding their afterglow characteristics, all the $Gd_2Hf_2O_7$ crystals show similar afterglow levels after X-ray irradiation for 2 ms.

1. Introduction

Scintillators are phosphors that immediately convert absorbed high-energy photons[1] or particles[2,3] into numerous UV–visible photons, and they have been utilized in many fields of radiation detection such as medical imaging,[4] security,[5] astrophysics,[6] and geophysical resource exploration.[7] For X- or γ-ray detection, scintillators generally require high scintillation light yield (LY), short decay time, high energy resolution, large effective atomic number, high density, and low afterglow levels; however, since no developed scintillators satisfy all these requirements, users must select a suitable one from existing scintillators. Thus, many researchers have made effort to search and develop new desirable materials.

In particular, a large effective atomic number and a high density provide a high interaction probability between materials and ionizing radiations,[8] so pyrochlore rare-earth hafnate is one of the potential choices as scintillators with high density (7.93–9.95 g/cm^3)[9] and large effective atomic number (Z_{eff} = 64–69).[10] For scintillator applications, some pyrochlore rare-earth hafnates have been investigated only in a polycrystalline form including ceramics and powders.[11–15] In general, scintillators have been developed in the single crystal form owing to the high optical transparency and homogeneity; however, the growing need is the driving force of developing new scintillators. In the case of rare-earth hafnate, since crystal growth is quite difficult because of the high melting point (~2400 °C), few studies on the growth of pyrochlore rare-earth hafnate compounds have been reported.[16–18] Previously, we introduced the optical floating zone (FZ) method as an effective and powerful technique for searching new

*Corresponding author: e-mail: nakauchi@ms.naist.jp
https://doi.org/10.18494/SAM.2020.2751

ISSN 0914-4935

oxide scintillators with high melting points.[19–23] Up to now, pyrochlore $RE_2Hf_2O_7$ (RE = La, Gd, Lu) single crystals have been prepared using an optical FZ furnace equipped with Xe lamps, and the scintillation properties of these single crystals were reported for the first time by Nakauchi *et al.*[18]

To improve scintillation characteristics by increasing oxygen vacancies, Zr and Ti ions with radii smaller than that of the Hf ion are introduced into $RE_2Hf_2O_7$ single crystals to distort the crystal lattice because Hf-based oxide materials typically show luminescence due to oxygen vacancies such as F and F^+ centers.[24,25] Such investigations have been performed for several scintillator candidates showing intrinsic luminescence, and activation has been achieved in intrinsic scintillators.[26] Enhancements by the substitution of homologous ions were also observed in $La_2Hf_2O_7$, and Zr and Ti ions improved the scintillation LY.[27] In this paper, we focus on such an enhancement effect in pyrochlore $Gd_2Hf_2O_7$.

2. Materials and Methods

Before crystal growth, undoped, 1% Zr-doped, and 1% Ti-doped $Gd_2Hf_2O_7$ polycrystalline rods were synthesized by conventional solid-state reaction. First, raw powders of ZrO_2 (99.99%, Furuuchi Chemical), TiO_2 (99.99%, High Purity Chemicals), Gd_2O_3 (99.99%, Furuuchi Chemical), and HfO_2 (99.95%, Furuuchi Chemical) were mixed. Then, the homogeneously mixed powder was formed into cylinder rods by applying hydrostatic pressure. Furthermore, the obtained rods were heated at 1500 °C for 8 h in air. After that, crystal growth was performed by the optical FZ technique (FZ-T-12000-X-VPO-PC-YH, Crystal Systems).[18] Here, the pulling-down and rotation rates were 30 mm/h and 3 rpm, respectively. To clarify the crystalline phase of the samples, the powder X-ray diffraction (XRD) pattern was measured using a diffractometer (MiniFlex600, Rigaku) over the 2θ range from 5 to 90º.

To determine the scintillation properties of the samples, scintillation spectra under X-ray irradiation were measured using our original setup.[28] The X-ray generator (XRB80N100/CB, Spellman) was equipped with an X-ray tube having a W anode target and a Be window. The X-ray tube was operated at a bias voltage of 80 kV and a tube current of 1.2 mA. In these analyses, the emitted scintillation photons from the samples were led to a spectrometer unit equipped with a CCD (DU-420-BU2, Andor) and a monochromator (Shamrock163, Andor) through an optical fiber. Here, the detector was cooled to 188 K using a Peltier module to reduce the thermal noise. Scintillation decay and afterglow curves were measured using an afterglow characterization system,[29] and the photomultiplier tube (PMT) covered the spectral range from 160 to 650 nm. In these analyses, the decay time constant was calculated by least-squares fitting with the sum of two exponential decay functions. To measure pulse height spectra, a sample covered with four layers of Teflon reflectors was mounted on the window of the PMT (R7600-200, Hamamatsu Photonics). The scintillation signals were converted to electrical signals, which were processed by the preamplifier (113, ORTEC), shaping amplifier (570, ORTEC), and multichannel analyzer (Pocket MCA 8000A, Amptek). Here, the shaping times for the synthesized samples and reference GS20 sample[30] were 2 and 0.5 μs, respectively.

3. Results and Discussion

All the $Gd_2Hf_2O_7$ single crystals were successfully obtained, and the typical sizes of the as-prepared samples were 5–6 mm ⌀ × 15 mm. Figure 1 shows the powder XRD patterns of the $Gd_2Hf_2O_7$ single crystals. Compared with the reference pattern,[14,31] only a single phase of $Gd_2Hf_2O_7$ with a cubic structure and a space group of $Fd\bar{3}m$ was observed. As illustrated in Fig. 2, the samples were cut into small pieces with sizes of 5–6 mm ⌀ × 3–5 mm thickness, and the top and bottom surfaces were polished to measure the luminescence properties.

Figure 3 shows the X-ray-induced scintillation spectra, and all the crystals exhibit scintillation signals with a broad peak at 510 nm. Although the emission origins have not been reported, we consider that the emission originated from oxygen vacancies related to an interpenetrating network of GdO_8 and HfO_6, as suggested in the case of $La_2Hf_2O_7$.[11,12] The X-ray-induced scintillation decay curves are illustrated in Fig. 4, and the obtained curves are approximated by the sum of two exponential functions having decay time constants of 50–60 ns (~80%) and 600–900 ns (~20%). The values are similar to those reported for a polycrystalline form.[11] The decay of the primary component is faster than that of a $Bi_4Ge_3O_{12}$ scintillator.

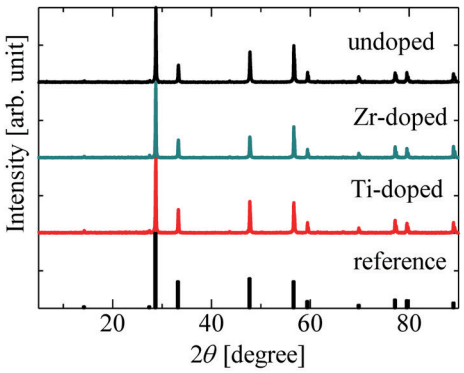

Fig. 1. (Color online) Powder XRD patterns of synthesized $Gd_2Hf_2O_7$ single crystals.

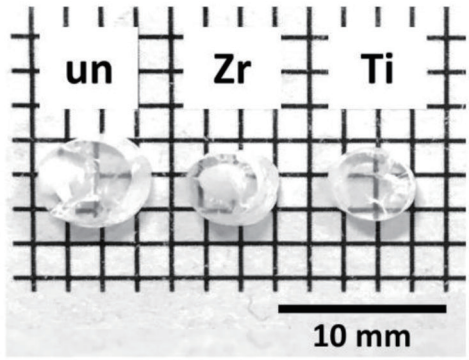

Fig. 2. (Color online) Photographs of synthesized $Gd_2Hf_2O_7$ single crystals.

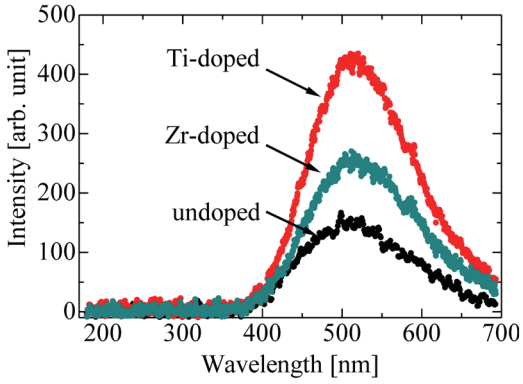

Fig. 3. (Color online) X-ray-induced scintillation spectra of $Gd_2Hf_2O_7$ single crystals.

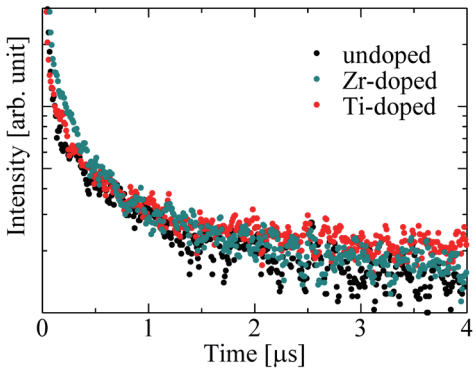

Fig. 4. (Color online) X-ray-induced decay time profiles of $Gd_2Hf_2O_7$ single crystals.

Table 1
Decay time constants calculated from decay curves. The values and standard deviations were calculated from results of five measurements.

Samples	τ_1 (ns)	τ_2 (ns)
Undoped	54 ± 9 (81%)	817 ± 186 (19%)
Zr-doped	53 ± 8 (85%)	662 ± 129 (15%)
Ti-doped	50 ± 9 (86%)	603 ± 190 (16%)

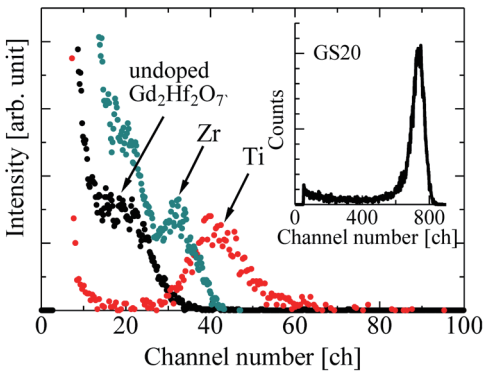

Fig. 5. (Color online) Pulse height spectra measured using $Gd_2Hf_2O_7$ under ^{241}Am α-ray (5.4 MeV) irradiation.

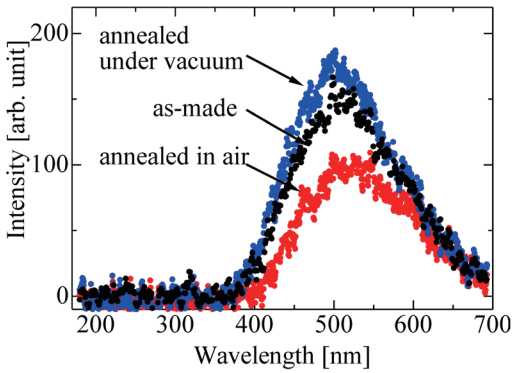

Fig. 6. (Color online) Scintillation spectra of undoped $Gd_2Hf_2O_7$ before (black) and after annealing under vacuum (blue) and in air (red).

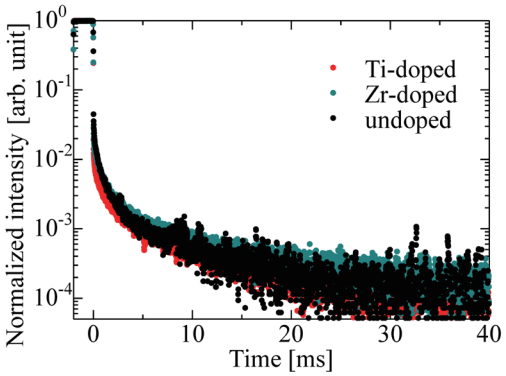

Fig. 7. (Color online) Afterglow curves of $Gd_2Hf_2O_7$ single crystals after 2 ms X-ray irradiation.

Figure 5 shows the pulse height spectra of the $Gd_2Hf_2O_7$ samples measured under ^{241}Am α-ray (5.4 MeV), and full energy peaks can be observed in all the samples. In comparison with the channel of the observed full energy peak of the GS20 scintillator showing an LY of 4000 photons/MeV,[30] the scintillation LYs of the undoped, Zr-doped, and Ti-doped $Gd_2Hf_2O_7$ samples are respectively 140, 280, and 210 photons/MeV with a typical error of ±10%. Since both Zr- and Ti-doped samples show higher scintillation LYs than the undoped one, the Zr and Ti doping processes appear to enhance the scintillation output.

To prove the emission origin, X-ray-induced scintillation spectra were measured using the samples annealed under vacuum and in air, as illustrated in Fig. 6. The sample annealed in air shows a small peak shift to a wavelength longer than that in the case of the as-prepared sample. Although it is difficult to control oxygen defects by such a simple annealing process, this result suggests that at least the obtained emissions include those derived from oxygen defects such as F and F^+ centers as well as the other Hf-based oxides.[24,25]

The afterglow curves of samples with 2 ms X-ray irradiation are shown in Fig. 7. The afterglow levels are calculated from $100 \times (I_2 - I_{BG})/(I_1 - I_{BG})$, where I_{BG}, I_1, and I_2 are defined as the background signal intensity, the signal intensity during irradiation, and the signal

intensity at t = 20 ms, respectively. The obtained afterglow levels of the undoped, Zr-doped, and Ti-doped crystals are 246, 346, and 236 ppm, respectively. All the samples exhibit similiar values, but the Ti-doped one exhibits the best afterglow level. The values are close to that of Tl:CsI (~300 ppm)[29] but higher than those of commercial oxide scintillators such as Ce:Gd_2SiO_5 (5.9 ppm).[32]

4. Conclusions

In this study, we focused on pyrochlore $Gd_2Hf_2O_7$ as a scintillator candidate with high density. Undoped, Zr-doped, and Ti-doped $Gd_2Hf_2O_7$ single crystals were successfully synthesized by the optical FZ technique. All the samples exhibit scintillation with a broad emission band at 550 nm, and the results suggest that the origin of the emission is oxygen vacancies, because annealing in air affects the spectral shape. The doped samples show higher scintillation LYs than the undoped one, indicating that both Zr and Ti improve the scintillation properties of $Gd_2Hf_2O_7$.

Acknowledgments

This work was supported by Grants-in-Aid for Scientific Research A (17H01375), Scientific Research B (18H03468), and JSPS Research Fellow (17J09488) from JSPS. The Cooperative Research Project of Research Institute of Electronics in Shizuoka University, NSG Foundation, Iketani Science and Technology Foundation, and NAIST Foundation are also acknowledged.

References

1 Y. Fujimoto, K. Saeki, D. Nakauchi, T. Yanagida, M. Koshimizu, and K. Asai: Sens. Mater. **31** (2019) 1241. https://doi.org/10.18494/SAM.2019.2183
2 M. Koshimizu, T. Yanagida, R. Kamishima, Y. Fujimoto, and K. Asai: Sens. Mater. **31** (2019) 1233. https://doi.org/10.18494/SAM.2019.2182
3 N. Kawaguchi, H. Kimura, M. Akatsuka, G. Okada, N. Kawano, K. Fukuda, and T. Yanagida: Sens. Mater. **30** (2018) 1585. https://doi.org/10.18494/SAM.2018.1926
4 L. Pidol, A. Khan-Harari, B. Viana, B. Ferrand, P. Dorenbos, J. T. M. de Haas, C. W. E. van Eijk, and E. Virey: J. Phys. Condens. Matter **15** (2003) 2091. https://doi.org/10.1088/0953-8984/15/12/326
5 J. Glodo, Y. Wang, R. Shawgo, C. Brecher, R. H. Hawrami, J. Tower, and K. S. Shah: Physics Procedia **90** (2017) 285. https://doi.org/10.1016/j.phpro.2017.09.012
6 T. Itoh, T. Yanagida, M. Kokubun, M. Sato, R. Miyawaki, K. Makishima, T. Takashima, T. Tanaka, K. Nakazawa, T. Takahashi, N. Shimura, and H. Ishibashi: Nucl. Instrum. Methods Phys. Res., Sect. A **579** (2007) 239. https://doi.org/10.1016/j.nima.2007.04.144
7 C. L. Melcher: Nucl. Instrum. Methods Phys. Res., Sect. B **40–41** (1989) 1214. https://doi.org/10.1016/0168-583X(89)90622-8
8 Y. Fujimoto, K. Saeki, D. Nakauchi, T. Yanagida, M. Koshimizu, and K. Asai: Sens. Mater. **30** (2018) 1577. https://doi.org/10.18494/SAM.2018.1927
9 M. J. Weber and R. R. Monchamp: J. Appl. Phys. **44** (1973) 5495. https://doi.org/10.1063/1.1662183
10 L. H. Brixner and E. Station: Mater. Res. Bull. **19** (1984) 143. https://doi.org/10.1016/0025-5408(84)90084-9
11 Y. Eagleman, M. Weber, and S. Derenzo: J. Lumin. **137** (2013) 93. https://doi.org/10.1016/j.jlumin.2012.10.034
12 Y. Eagleman, M. Weber, A. Chaudhry, and S. Derenzo: J. Lumin. **132** (2012) 2889. https://doi.org/10.1016/j.jlumin.2012.06.002
13 K. Wahid, M. Pokhrel, and Y. Mao: J. Solid State Chem. **245** (2017) 89. https://doi.org/10.1016/j.jssc.2016.10.004

14 J. Trojan-Piegza, S. Gierlotka, E. Zych, and W. Lojkowski: J. Am. Ceram. Soc. **97** (2014) 1595. https://doi.org/10.1111/jace.12788
15 Y. Ji, D. Jiang, and J. Shi: J. Mater. Res. **20** (2005) 567. https://doi.org/10.1557/JMR.2005.0073
16 J. Chun, P. G. Reuvekamp, D. Chen, C. Lin, and R. K. Kremer: J. Mater. Chem. C **3** (2015) 491. https://doi.org/10.1039/C4TC02416H
17 M. C. Hatnean, R. Sibille, M. R. Lees, M. Kenzelmann, V. Ban, V. Pomjakushin, and G. Balakrishnan: J. Phys. Condens. Matter **29** (2017) 075902. https://doi.org/10.1088/1361-648X/29/7/075902
18 D. Nakauchi, G. Okada, N. Kawaguchi, and T. Yanagida: Jpn. J. Appl. Phys. **57** (2018) 100307. https://doi.org/10.7567/JJAP.57.100307
19 M. Akatsuka, Y. Usui, D. Nakauchi, G. Okada, N. Kawaguchi, and T. Yanagida: Sens. Mater. **30** (2018) 1525. https://doi.org/10.18494/SAM.2018.1922
20 G. Okada, M. Akatsuka, H. Kimura, M. Mori, N. Kawano, N. Kawaguchi, and T. Yanagida: Sens. Mater. **30** (2018) 1547. https://doi.org/10.18494/SAM.2018.1919
21 D. Nakauchi, N. Kawaguchi, and T. Yanagida: Sens. Mater. **31** (2019) 1249. https://doi.org/10.18494/SAM.2019.2184
22 H. Fukushima, D. Nakauchi, N. Kawaguchi, and T. Yanagida: Sens. Mater. **31** (2019) 1273. https://doi.org/10.18494/SAM.2019.2187
23 M. Akatsuka, D. Nakauchi, N. Kawaguchi, and T. Yanagida: Sens. Mater. **31** (2019) 1289. https://doi.org/10.18494/SAM.2019.2189
24 N. Umezawa, K. Shiraishi, T. Ohno, M. Boero, H. Watanabe, and T. Chikyow: Phys. B **376–377** (2006) 392. https://doi.org/10.1016/j.physb.2005.12.101
25 K. Tse, D. Liu, K. Xiong, and J. Robertson: Microelectron. Eng. **84** (2007) 2028. https://doi.org/10.1016/j.mee.2007.04.020
26 P. Brinckmann: Phys. Lett. **15** (1965) 304
27 D. Nakauchi, N. Kawaguchi, and T. Yanagida: Opt. Mater. **90** (2019) 227. https://doi.org/10.1016/j.optmat.2019.02.050
28 T. Yanagida, K. Kamada, Y. Fujimoto, H. Yagi, and T. Yanagitani: Opt. Mater. **35** (2013) 2480. https://doi.org/10.1016/j.optmat.2013.07.002
29 T. Yanagida, Y. Fujimoto, T. Ito, K. Uchiyama, and K. Mori: Appl. Phys. Express **7** (2014) 062401. https://doi.org/10.7567/APEX.7.062401
30 C. W. E. van Eijk: Nucl. Instrum. Methods Phys. Res., Sect. A **460** (2001) 1. https://doi.org/10.1016/S0168-9002(00)01088-3
31 Y. Xu, M. Yamazaki, and P. Villars: Jpn. J. Appl. Phys. **50** (2011) 11RH02. https://doi.org/10.1143/JJAP.50.11RH02
32 D. Nakauchi, N. Kawano, N. Kawaguchi, and T. Yanagida: Jpn. J. Appl. Phys. **59** (2020) SCCB04. https://doi.org/10.7567/1347-4065/ab515d